引用格式：LIU Zhihai, LUO Binbin, WU Decao, et al. Research on Traditional Chinese Medicine Pulse Diagnosis Based on Three Channel U-shaped Micro Nano Fiber Pulse Sensor[J]. Acta Photonica Sinica, 2026, 55(1):0106006
刘志海,罗彬彬,吴德操,等.基于三通道U型微纳光纤脉搏传感器的中医脉诊研究[J].光子学报,2026,55(1):0106006

基于三通道U型微纳光纤脉搏传感器的中医脉诊研究

刘志海,罗彬彬,吴德操,邹雪,李昆,黄嵊釉,胡新宇
(重庆理工大学 光纤传感与光电检测重庆市重点实验室,重庆 400054)

摘　要:为实现中医脉诊从主观经验向客观量化的转变,提出一种基于三通道U型微纳光纤的柔性传感器及系统。该传感器根据中医的手指把脉模式,将三个U型微纳光纤嵌入双层聚二甲基硅氧烷薄膜,并集成于聚碳酸酯基板,其三通道设计能够同步采集寸、关、尺三部在不同按压深度(浮、中、沉)下的脉搏波数据,模拟传统脉诊中的“三部九侯”。结果表明,三个通道的微纳光纤传感单元具备高灵敏度(11.49% kPa^{-1}、11.64% kPa^{-1}和11.13% kPa^{-1})、快速响应与恢复时间(22.7 ms/9.4 ms、31.2 ms/10.6 ms和29.8 ms/8.5 ms)以及良好的一致性、重复性和稳定性等特点。进一步,结合一维卷积神经网络和双向门控循环单元深度学习模型,对多深度脉搏波数据进行量化分析,实现对左右手典型脉象的分类,准确率分别达到96.61%和96.07%。本研究可为中医脉诊的客观化、数字化与智能化提供新的方案。

关键词:光纤传感器;微纳光纤;中医脉诊;脉象识别;三通道
中图分类号:TN253　　**文献标识码**:A　　**doi**:10.3788/gzxb20265501.0106006

0　引言

中医脉诊是一种传统的健康评估方法,通过触诊桡动脉脉搏特征,判断气血运行及脏腑功能的变化[1-2]。传统脉诊依赖医生的主观经验,其诊断标准难以统一,客观性受到质疑,因此,脉诊的数字化和客观化成为发展趋势[3]。为克服上述问题,许多学者通过传感器采集脉搏波信号,以实现更为客观的健康评估。电学类柔性触压传感器是常用的脉搏波信号采集方案,但存在易受寄生效应、信号串扰和电磁噪声影响等问题[4-8],从而影响诊断准确性。

光纤传感器因高灵敏度和抗电磁干扰特性,在生理参数检测领域备受关注,其中,微纳光纤(Micro-Nano Fiber, MNF)具有微尺寸、强倏逝场及柔韧性好的优势,十分适合于制备柔性传感器。目前,许多学者将基于MNF的柔性传感器应用于脉搏检测等领域。例如,2018年,LI Jihong等[9]提出一种基于谐振环MNF的可穿戴脉搏波传感器,其具备高灵敏度和快速响应的能力,能够实时监测脉搏波、呼吸等生理信号。2020年,PAN Jing等[10]提出一种将0.8 μm直径的MNF嵌入聚二甲基硅氧烷(Polydimethylsiloxane, PDMS)薄层的光学仿生皮肤,获得超高的压力灵敏度(1 870 kPa^{-1})、极低的检测限(7 mPa)以及超快的响应时间(10 μs),能灵敏感知手腕的微弱脉搏。2023年,LI Liangye等[11]提出一种可穿戴的无对准微光纤传感器芯片(Alignment-Free Microfiber Sensor Chip, AFMSC),由U型MNF与柔性液囊构成,可用于持续监测心血管相关的生理参数。2023年,邹雪等[12]提出一种基于反射式MNF耦合器的高灵敏度传感膜片,可无须精准对准获取脉搏信号,结合双通道检测与支持向量回归,实现基于脉搏传导时间的无创血压预测。2024年,

基金项目:重庆市自然科学基金创新发展联合基金(CSTB2023NSCQ-LZX0008),重庆市教委科学技术研究项目(KJQN202401103),国家市场监管重点实验室开放课题(CQTJ-XBJD-KFKT202302),重庆理工大学创新团队(2023TDZ002),重庆理工大学重大科研项目同步开展基础及应用基础项目(2024TBZ027)
第一作者:刘志海,2418349625@qq.com
通讯作者:罗彬彬,luobinbin@cqut.edu.cn
收稿日期:2025-08-13;**录用日期**:2025-09-19

CHEN Zongyu等[13]设计一种三维光纤触觉传感器，由嵌入PDMS中的弧形微型光纤光栅阵列构成，通过检测光强变化区分不同方向的力，获得0.01 N的分辨率和抗温度干扰特性，并应用于人体脉搏监测。尽管上述MNF传感器在灵敏度、生理参数识别及血压预测等方面取得显著进展，但目前多集中于单点或局部脉搏信号的采集，难以满足中医脉诊对寸、关、尺三部位脉象同步感知的需求。同时，现有研究多侧重于脉搏信号的获取与初步特征提取，对于中医脉象多维特征的量化表达、辨识机制及其在智能化脉诊中的应用研究仍显不足。

为此，本文提出一种基于三通道U型MNF传感器的中医脉诊传感系统，通过将三个一致性良好的U型MNF嵌入PDMS薄膜并固定在聚碳酸酯(Polycarbonate，PC)板上，模拟中医诊脉的模式，能够同步采集寸、关、尺三部位在不同按压深度(浮、中、沉)下的脉搏信号，全面捕捉脉搏波形的细微变化，并进行量化分析；通过结合一维卷积神经网络(1D-Convolutional Neural Network，1D-CNN)与双向门控循环单元(Bidirectional Gated Recurrent Unit，BiGRU)模型，对左右手典型脉象进行精准分类识别。

1 原理与设计

1.1 三通道脉搏传感器设计

中医脉诊的核心在于通过三根手指感知桡动脉的脉搏特征，以判断气血运行和脏腑功能的状态[14]，如图1(a)所示。根据中医脉诊的模式，构建如图1(b)所示的三通道脉搏波传感器，采用独立的单元设计，分别置于寸、关、尺三脉位，以避免传感单元间的相互干扰，实现中医脉搏信号的同步检测。图1(c)为分层结构的U型MNF脉搏传感单元，由三层组成：外层PDMS薄膜直接贴合皮肤，凭借其弹性与柔韧性，精准感知微小压力与形变；中间PDMS层封装并保护MNF；下层PC板提供支撑，确保传感器的稳定性和耐用性。脉搏波引起的压力作用于外层PDMS，导致MNF弯曲形变，进而调制透射光强度。

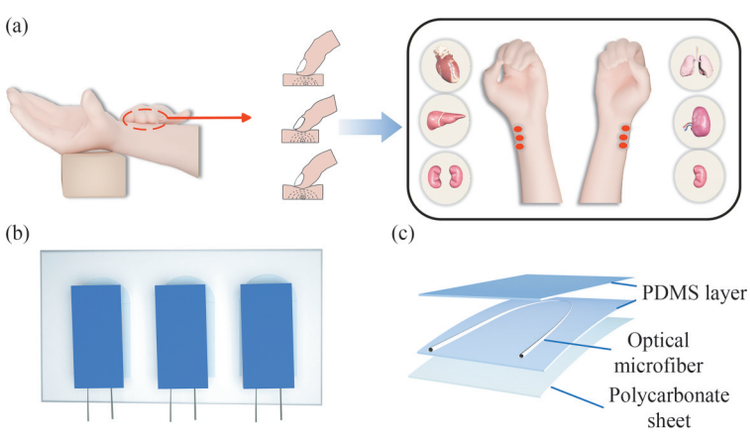


图1 模拟中医脉诊的柔性传感器。(a)中医“三部九候”脉诊示意图；(b)用于中医脉诊的三通道MNF传感器；(c)U型MNF脉搏传感单元

Fig. 1 Flexible sensor for simulating pulse diagnosis in Traditional Chinese Medicine (TCM). (a) Schematic diagram of the “Three Regions and Nine Positions” pulse diagnosis in TCM; (b) Tri-channel MNF sensor for TCM pulse diagnosis; (c) U-shaped MNF pulse sensor unit

1.2 U型MNF原理与设计

通过对单模光纤进行熔融拉锥处理，可以制备出锥形MNF，并弯曲呈U型后采用PDMS薄膜进行封装。据本课题组之前的研究[15]，此时PDMS可被视为MNF腰区的包层，而MNF腰区本身视为纤芯，当脉搏跳动时，封装的MNF会发生弯曲，导致纤芯与包层之间产生应变差异，进而引起有效折射率差和相位差的变化，最终导致透射率的改变。

通过有限元模拟软件COMSOL，对MNF基模的模场分布进行仿真，设定工作波长为1 550 nm，纤芯折射率为1.46，PDMS包层折射率为1.40。如图2(a)所示，当MNF弯曲半径(Radius of Curvature，ROC)为2 mm时，随着MNF直径从8 μm减小到1 μm，倏逝场能量占比从约7.2%增强至约94.4%。图2(b)表明，当MNF直径为3 μm时，随着弯曲半径从4 mm减小到0.1 mm，倏逝场能量占比从约63%增加到约85.9%。尽管较小的MNF直径和弯曲半径有助于增强光场能量的泄漏，提高灵敏度，但会降低机械强度，增加断裂风

险。为平衡倏逝场效应与机械强度，同时适应桡动脉穴位脉搏跳动的有效半径（约2.5～5 mm），选用直径为3 μm、曲率半径为2 mm的MNF。该设计不仅确保传感器在检测脉搏时的稳定性，还能保证传感器与桡动脉良好贴合，从而提高检测的可靠性与准确性。

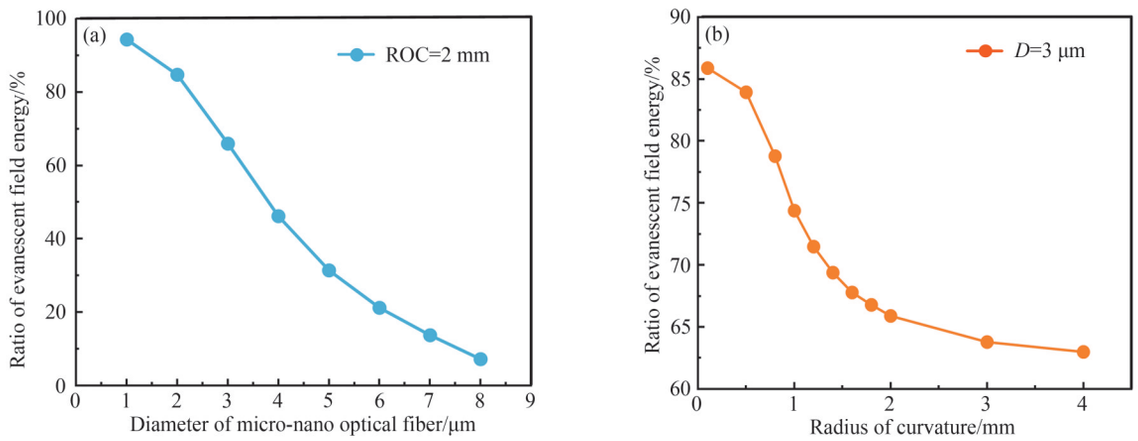


图2　MNF倏逝场占比仿真。(a)光纤直径对倏逝场能量占比的影响；(b)弯曲半径对倏逝场能量占比的影响

Fig. 2　Simulation of evanescent field proportion for MNF. (a) Effect of fiber diameter on the evanescent field energy ratio; (b) Effect of bending radius on the evanescent field energy ratio

1.3　传感器力学仿真分析

为深入研究传感器的力学响应，采用ANSYS软件进行仿真分析。材料参数如下：PDMS薄膜密度ρ=980 kg/m^3，泊松比ν=0.48，杨氏模量E=2.5 MPa；MNF密度ρ=1 857 kg/m^3，泊松比ν=0.154 3，杨氏模量E=26.4 GPa；PC板密度ρ=1 900 kg/m^3，泊松比ν=0.136，杨氏模量E=24.6 GPa。封装结构中PDMS上下层厚度对传感器性能具有显著影响。据研究[16]，较薄的上层PDMS厚度可显著增大MNF的平面应力，而下层PDMS的影响相对较小。针对脉搏传感应用，传感器需要对微弱压力变化具有高灵敏度，同时封装结构需具备必要的机械强度。因此，将外层PDMS膜厚度设定为100 μm，以平衡灵敏度与结构韧性；中间PDMS层和PC板的厚度均为100 μm，以提供稳定支撑；MNF的曲率半径设置为2 mm，直径设置为6 μm，该直径接近ANSYS可解析的最小几何尺度，既能有效捕捉其弯曲应变，又兼顾仿真精度与合理性。

在外层PDMS薄膜层选取约4 mm×4 mm的不规则区域，如图3(a)，模拟MNF传感器与桡动脉之间的

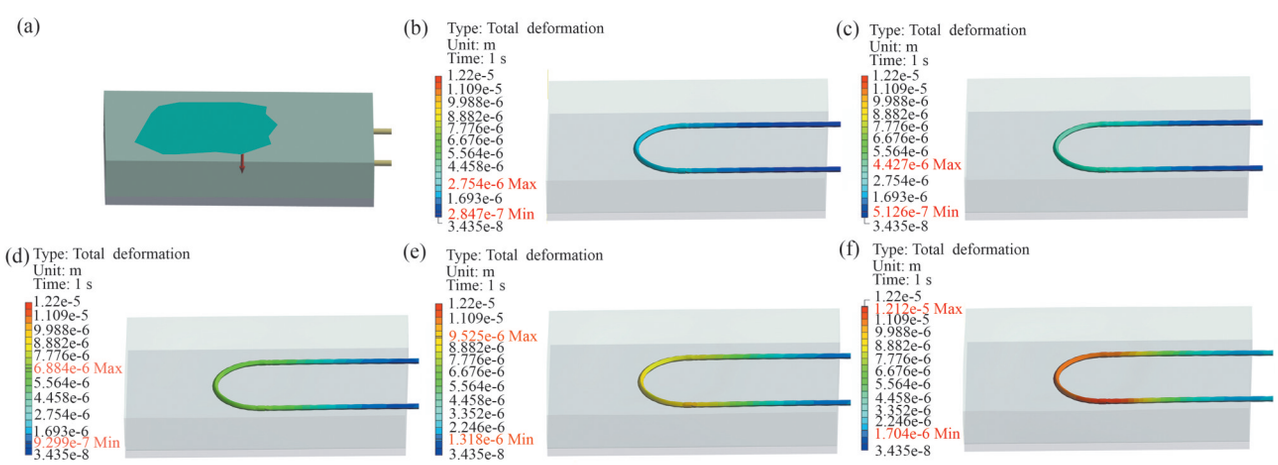


图3　U型MNF力学仿真。(a)PDMS薄膜外层的不规则接触区域；(b)压头载荷F=0.1 N下的形变云图；(c)压头载荷F=0.2 N下的形变云图；(d)压头载荷F=0.4 N下的形变云图；(e)压头载荷F=0.6 N下的形变云图；(f)压头载荷F=0.8 N下的形变云图

Fig. 3　Mechanical simulation of the U-shaped MNF. (a) Irregular contact areas of the outer PDMS film layer; (b) Deformation contour under an indenter load of F=0.1 N; (c) Deformation contour under an indenter load of F=0.2 N; (d) Deformation contour under an indenter load of F=0.4 N; (e) Deformation contour under an indenter load of F=0.6 N; (f) Deformation contour under an indenter load of F=0.8 N

实际接触状态。为评估其性能，在该区域施加0.1 N、0.2 N、0.4 N、0.6 N和0.8 N的法向压力，此范围涵盖人体的正常脉搏压力（约0.2～0.7 N）。如图3(b)～(f)所示，随着压力增大，U型MNF弯曲程度呈现递增趋势，最大形变量从0.1 N的2.754×10^{-6} m增加至0.8 N的1.212×10^{-5} m，其中，U型MNF的中心区域对压力变化高度敏感，表明传感器对微小力学变化具有高灵敏度，适用于脉搏监测等应用。在实际中，由高温拉锥工艺制备的MNF直径（约3 μm）小于仿真模型的6 μm，因此，可推断其对表面微观力学变化更为敏感，具有更高的压力灵敏度。

1.4 传感器制备

采用火焰熔融拉锥法与SM28单模光纤制备U型MNF[17]。在真空吸附台上，光纤拉锥机的氢气流速设置为225 sccm，预绘制速度为120 μm/s，预拉制长度为13 500 μm。拉锥过程中，通过实时监控光谱干涉峰的自由光谱范围（Free Spectral Range，FSR），可精确调控光纤直径[18]。图4(a)为三个制备的MNF，直径分别为2.918 μm、2.747 μm、3.090 μm，U型MNF的弯曲半径分别为2.029 mm、2.007 mm、2.004 mm。

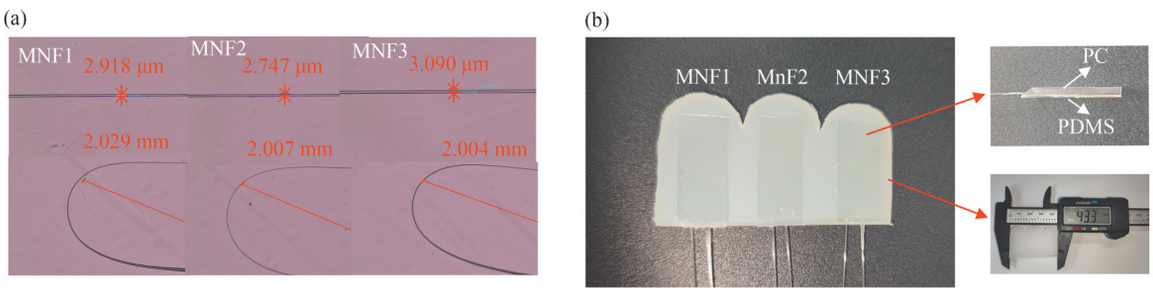


图4 三个U型MNF参数及传感器结构。(a)三个U型MNF的显微图像；(b)三通道MNF传感器实物结构

Fig. 4 Parameters of the three U-shaped MNFs and the structure of the tri-channel MNF sensor. (a) Microscopic images of the three U-shaped MNFs; (b) Physical structure of the tri-channel MNF sensor

三通道触觉传感器的集成过程如下：首先，将三个制备好的U型MNF封装在两层厚度为100 μm的PDMS薄膜之间，并使用液体PDMS作为粘合剂；接着，采用液体PDMS将PC板粘附在PDMS层的外表面，在50 ℃下固化1 h以消除气泡，形成三个U型MNF单元；随后，利用3D打印技术制作模具，并注入液态硅胶，构成一个模拟三指触压分布的平台；最后，将三个U型MNF单元固定于硅胶平台内，完成中医脉诊三通道MNF传感器的集成，如图4(b)。

2 实验与讨论

2.1 力学性能实验及分析

如图5所示，使用放大自发辐射宽带光源（Amplified Spontaneous Emission Source，ASE，型号：CONQUER，波长范围：1 250～1 650 nm）作为光源，通过精密测力计（Manual Pressure Tester，MPT，型号：Mark-10 ESM303）依次对三通道传感器的三个U型MNF单元对应的外层PDMS膜施加静态和动态压力，由此产生的透射光强变化经3 dB耦合器分别传输至光谱分析仪（Optical Spectrum Analyzer，OSA，型号：Yokogawa AQ6370B，波长范围：600～1 700 nm）和光电探测器（Photodetector，PD，带宽：200 kHz）。光谱分析仪用于记录透射光谱的变化，光电探测器则将光强变化转换为电信号，并在示波器上输出显示。

图6(a)～(c)分别显示在1 520～1 620 nm波长范围内，MNF 1、MNF 2和MNF 3在不同压力水平（0～1 N增量为0.1 N，1～8 N增量为1 N）下的透射光谱，可见，随着压力的增加，MNF弯曲程度变大，倏逝场能量泄露增大，透射光谱强度逐渐下降，符合1.3节仿真分析的推断。在本实验中，传感器与压头的接触面积为2.44×10^{-4} m^2，根据压强计算公式$P=F/s$，F为垂直于物体的压力（N），可得传感器在0～8 N压力范围内对应的压强范围为0～32.8 kPa。

如图6(d)所示，随着精密测力仪逐步施加0～1.2 N（对应压强0～4.9 kPa）的静态压力（每个压力等级保持2 s）于传感器单元，三个通道的输出电压均随着压力增加而逐渐降低。图6(e)进一步展示三个通道输出电压相对变化（$\Delta V/V_0$，V_0为无压力下的初始输出强度）随压力变化的曲线，表明在0～1.7 N（对应压强0～

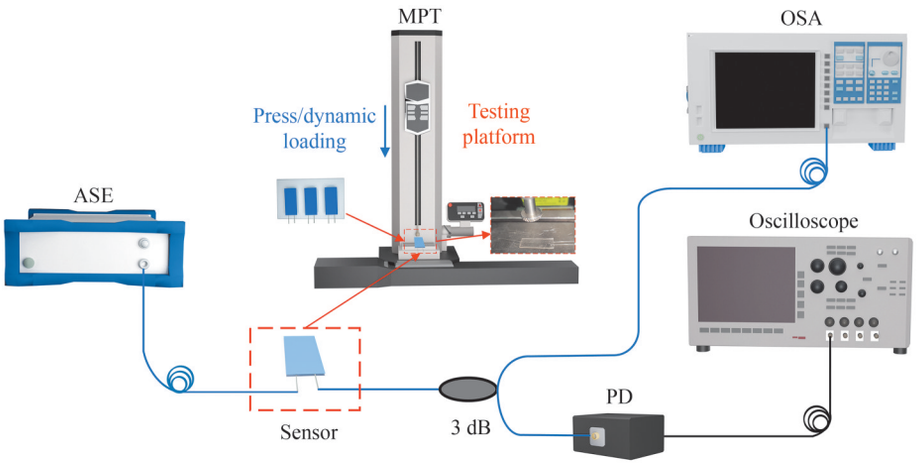


图5　力学性能测试实验系统

Fig. 5　Mechanical performance testing experimental system

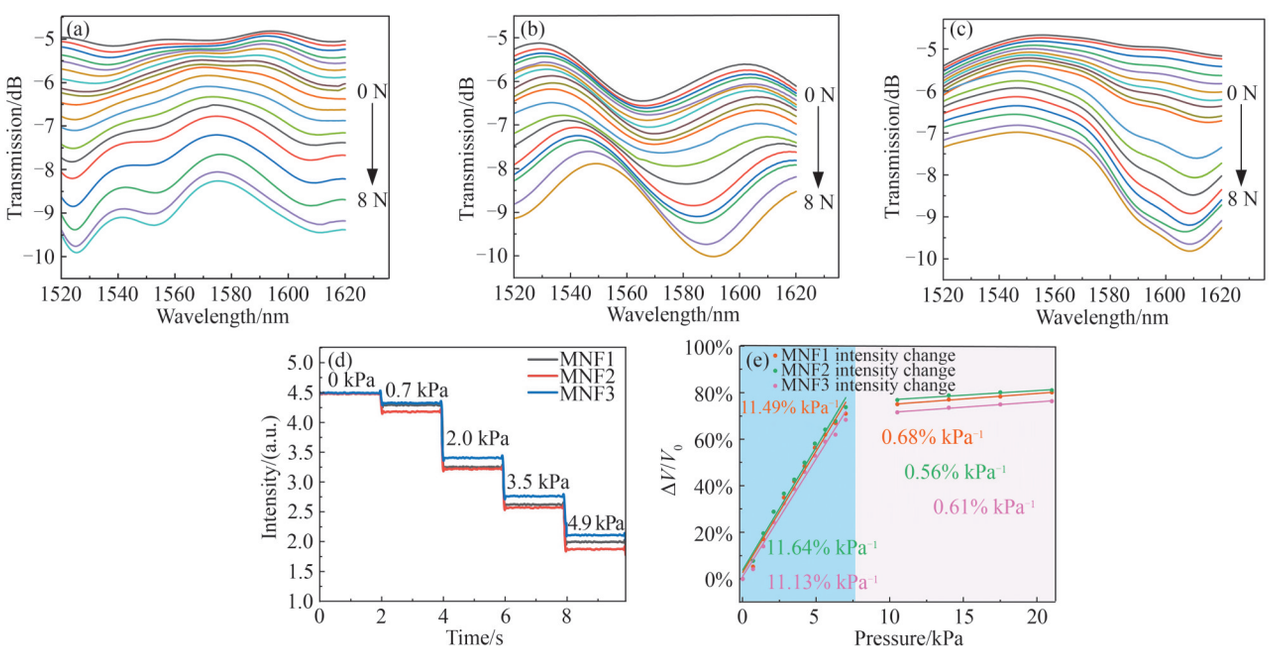


图6　力学性能测试结果。(a) MNF 1的光谱压力响应；(b) MNF 2的光谱压力响应；(c) MNF 3的光谱压力响应；(d)三通道的静压力响应；(e)三通道的压力灵敏度

Fig. 6　Results of the mechanical performance test. (a) Pressure response of MNF 1 spectrum; (b) Pressure response of MNF 2 spectrum; (c) Pressure response of MNF 3 spectrum; (d) Static force response of tri-channel; (e) Pressure sensitivity of tri-channel

7 kPa)范围内，传感器的灵敏度分别为11.49% kPa^{-1}、11.64% kPa^{-1}和11.13% kPa^{-1}；在1.7～5.1 N(对应压强7～21 kPa)范围内，灵敏度分别降低为0.68% kPa^{-1}、0.56% kPa^{-1}和0.61% kPa^{-1}。可见在低压力范围内(0～1.7 N)，三个传感通道表现出良好的灵敏度及较高的一致性，适合感知脉搏等微小压力信号。然而，由于制造工艺的微小差异，三个传感通道之间存在差异，最大相对差异约为4.6%，这些差异可能影响脉搏信号的幅值和波形精度，但通过算法校准补偿，可有效提升脉搏信号的感知精度。

进一步分析传感器对外部力加载和卸载的实时性，如图7(a)～(c)所示，在加载/卸载速率为80 μm/s、最大加载力为5 N、峰值处停0.6 s的条件下，MNF 1、MNF 2及MNF 3的响应时间和恢复时间分别为22.7 ms/9.4 ms、31.2 ms/10.6 ms和29.8 ms/8.5 ms，均具有快速响应和恢复能力。为评估传感器的长期稳定性，进行加载-卸载循环测试，经过600次循环后，传感器的三通道光信号输出仍保持稳定，如图7(d)，这主要得益于PDMS与PC对MNF的可靠封装，以及传感器多层结构的牢固结合。

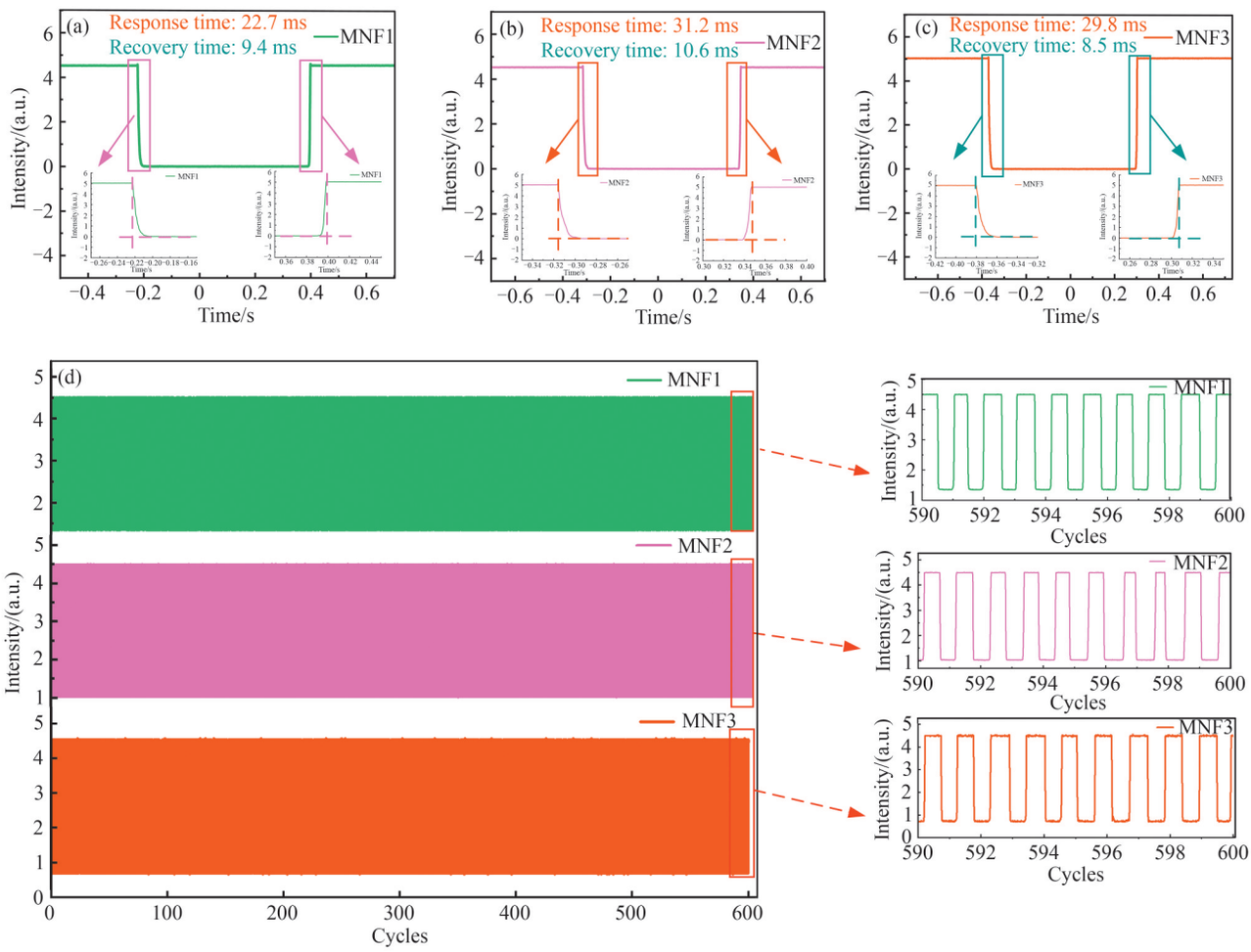


图7 三通道响应/恢复时间及稳定性分析。(a)MNF1的响应/恢复时间;(b)MNF2的响应/恢复时间;(c)MNF3的响应/恢复时间;(d)稳定性测试

Fig. 7 Tri-channel response/recovery time and stability analysis. (a) Response/recovery time of MNF 1; (b) Response/recovery time of MNF 2; (c) Response/recovery time of MNF 3; (d) Stability testing

表1对比本研究与已报道脉搏传感器的最大灵敏度、工作范围、响应/恢复时间、通道数等性能参数。可见,本传感器的灵敏度较高,压力检测范围可适应脉搏范围,重要的是三通道设计能够更全面地捕捉脉搏信号,可提升检测的准确性和可靠性。同时,所设计传感器的响应速度及恢复速度快,能有效捕捉微小脉搏引起的压力变化和瞬时频率波动。

表1 本传感器与其他脉搏检测传感器的性能比较

Table 1 Performance comparison between this sensor and other pulse detection sensors

Types of sensors	Package material	Highest sensitivity	Working range	Response time	Number of channels	References
Resistive sensor	Printed flexible	3.997 kPa^{-1}	0~100 kPa	120 ms/60 ms	1	[4]
Resistive sensor	Synthetic graphene	8.65% kPa^{-1}	0~12 kPa	100 ms/500 ms	3	[5]
Fiber optic sensor	PDMS/PMMA	0.22 kPa^{-1}	0~10.5 kPa	11 ms/48 ms	1	[11]
Fiber optic sensor	PDMS/PC	11.64% kPa^{-1}	0~32.8 kPa	22.7 ms/9.4 ms	3	This work

2.2 脉诊实验与讨论

基于三通道MNF传感器,构建如图8(a)所示的中医脉诊传感系统,采用ASE作为光源,并通过分光器(Optical Fiber Coupler, OFC)将输出光平均分配至三个MNF传感通道,将三通道传感器分别贴附于手腕桡侧“寸、关、尺”三脉位,实现多点脉搏信号的同步采集。三路传感通道的光信号通过三通道PD模块转换为电信号,由示波器实时显示各脉位的动态脉搏波形。

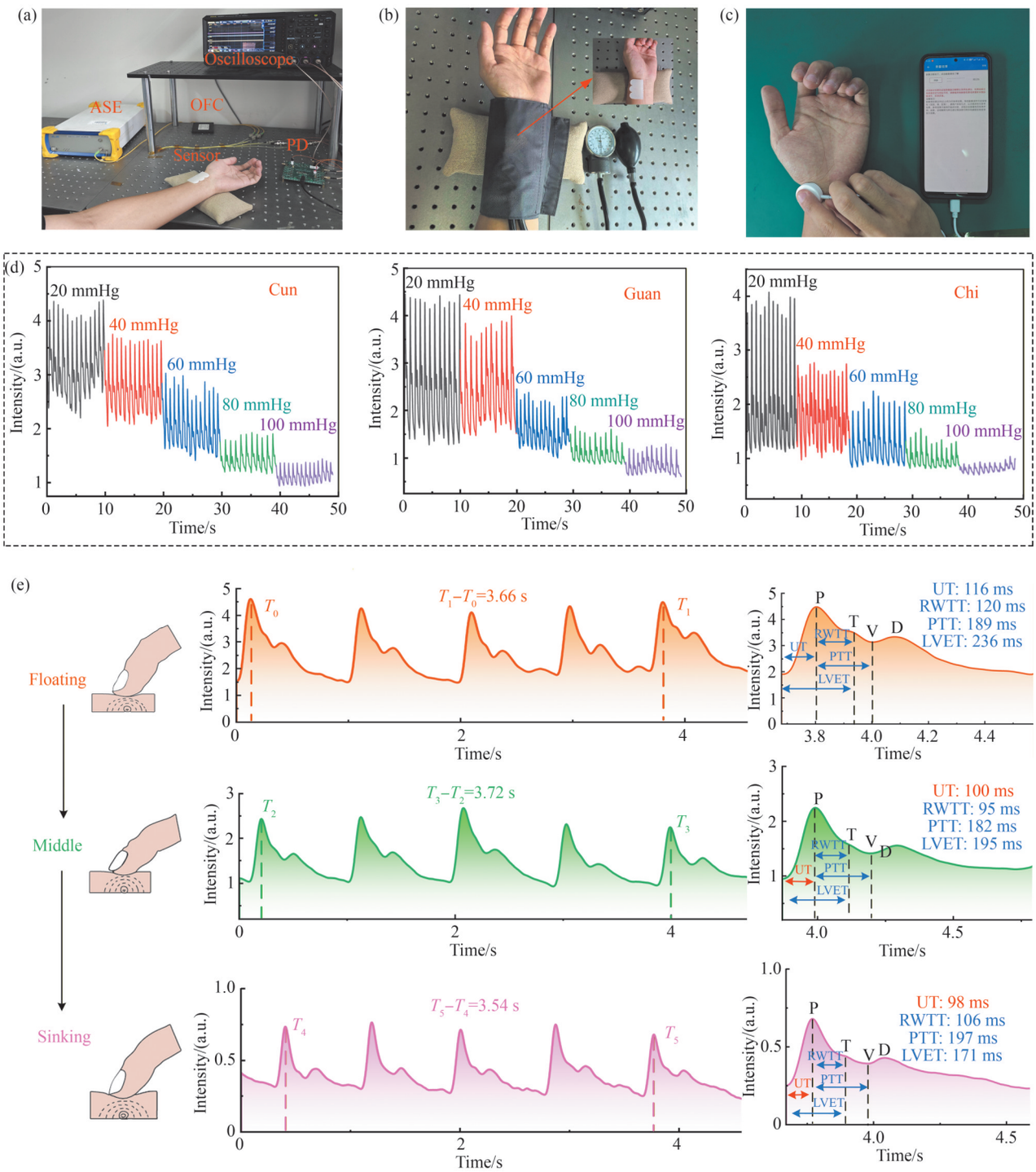


图8　中医脉诊系统设计与脉搏特征分析。(a)脉诊系统示意图；(b)基于充气式鱼跃袖带的脉象采集；(c)基于蓝骄AI诊断仪的脉象判别；(d)寸、关、尺三部位不同按压深度下的脉搏波变化；(e)寸部“浮、中、沉”三种脉象的脉搏波形特征

Fig. 8　Design of TCM Pulse Diagnosis System and Analysis of Pulse Characteristics. (a) Schematic diagram of the pulse diagnosis system; (b) Pulse collection based on inflatable Yuwell cuff; (c) Distinguishing pulse based on Blue Pride AI diagnostic instrument; (d) Pulse wave changes of cun, guan, and chi at different pressing depths; (e) Pulse waveform characteristics of "floating, middle and sinking" in the cun part

首先模拟中医脉诊“浮、中、沉”按压深度，探讨不同按压深度对脉搏信号特征的影响。如图8(b)所示，实验中，使三通道MNF传感器与桡动脉保持适形接触，通过可充气鱼跃袖带施加静态压力，模拟手指施加的不同压力，从而模拟中医脉诊中不同深度的按压；接着，如图8(c)所示，采用单通道蓝骄AI脉诊仪，依次

对“寸、关、尺”三部脉象进行检测，并结合其内部算法获得对应的脉象分类结果。图8(d)为在0至100 mmHg范围内(间隔20 mmHg)所采集的三部(寸、关、尺)脉搏信号。可见，随着压力增加，脉搏信号的幅度减小，这主要是由于压力增大导致MNF微弯程度增加，光传输损耗加剧，进而光强变化幅度趋于饱和，与图6(e)的测试结果一致。为便于对“浮、中、沉”进行定量分析，此处定义0～20 mmHg为“浮”，20～60 mmHg为“中”，60～80 mmHg为“沉”。

图8(e)左图展示寸部“浮、中、沉”按压深度下的施力示意及脉搏波，提取各按压深度下脉搏波的关键时间节点(T_0、T_1、T_2)及其间隔，标记脉搏周期中的主要特征点，如收缩期波峰(P)及舒张期的T、V、D点；进一步提取包括上升时间(Rise Wave Transit Time, RWTT)、收缩期波形持续时间(Upstroke Time, UT)、脉搏波传导时间(Pulse Transit Time, PTT)和左心室射血时间(Left Ventricular Ejection Time, LVET)特征参数，得到图8(e)右图对应的脉搏特征参数的结果。可见，随外部压力增加，波形趋于平坦，UT减小，上升速率加快，这主要是因为按压力度加深导致血管壁刚性增加、顺应性降低，从而加快脉搏波传播、使波形上升陡峭。此外，关部与尺部在不同按压深度下也呈现出与寸部相似的变化趋势，反映出三部穴位对按压响应的一致性，表明所设计的三通道MNF脉搏传感系统具有类似中医脉诊的良好脉搏感知能力。

进一步，基于蓝骄AI脉诊仪的分类结果，对三通道MNF传感器所采集到的脉搏波信号进行标注；随后，运用波形分析技术，从“数、形、势”三个维度对已标注的七种常见脉象(常、紧、滑、实、洪、细、数)进行定量分析[19]，并结合现代生理参数(UT、PTT、RWTT和LVET)深入探讨脉象变化的规律。具体来说，“数”代表脉搏频率，反映心率(Heart Rate, HR)特征；“形”对应脉搏波形，通过UT与RWTT度量其陡峭度，辅助识别洪脉、实脉、细脉等；“势”表征脉搏的力度与波动程度，结合PTT和LVET指标，评估血流动力学变化及心功能状态，从而帮助判别紧脉与滑脉等脉象，详细分析结果见表2。

表2 七种常见脉象的客观生理指标分析

Table 2 Analysis of objective physiological indicators of seven common pulse conditions

Pulse qualities	HR	UT / RWTT	PTT	LVET
Normal pulse	Normal (60～80 bpm)	Normal	Normal	Normal
Forceful pulse	Normal or Slightly Faster	Shortened/variable	Shortened	Normal or slightly longer
Rapid pulse	Faster (＞90 bpm)	Shortened	Normal or slightly shortened	Shortened
Flooding pulse	Faster (＞90 bpm)	Shortened/variable	Shortened	Normal or slightly longer
Slippery pulse	May be normal, faster, or slower	Normal or slightly longer	Normalor slightly longer	Normal or slightly longer
Tense pulse	May be normal, faster, or slower	Shortened/variable	Normal or shortened	Normal or slightly shortened
Thready pulse	May be normal, faster, or slower	Normal or slightly longer	Normal or slightly longer	Normal or slightly longer

通过结合不同脉象与病例分析，进一步表征其临床意义，比如：志愿者1腹泻时，左手关部脉象呈细脉，如图9(a)，符合气血亏虚、脾胃虚弱的病理机制；康复后，脉象恢复为常脉，如图9(b)；志愿者3感冒时，左手寸部脉象呈紧脉，如图9(c)，与寒邪束表、卫阳郁闭的病机一致；女性志愿者5生理期时，左手寸部脉象呈滑脉，如图9(d)，提示经血充盛，生理期后脉象转为细脉，反映气血耗损；志愿者6咳嗽、咽喉干燥时，右手寸部脉象呈数脉，如图9(e)，与风热犯肺病机一致；值得一提的是，图9(a)～(e)均选择的是中候脉搏波进行分析，这是由于中候波形最为稳定，相对于浮候、沉候能准确地反映脉象的真实变化，便于临床分析与标准化研究。

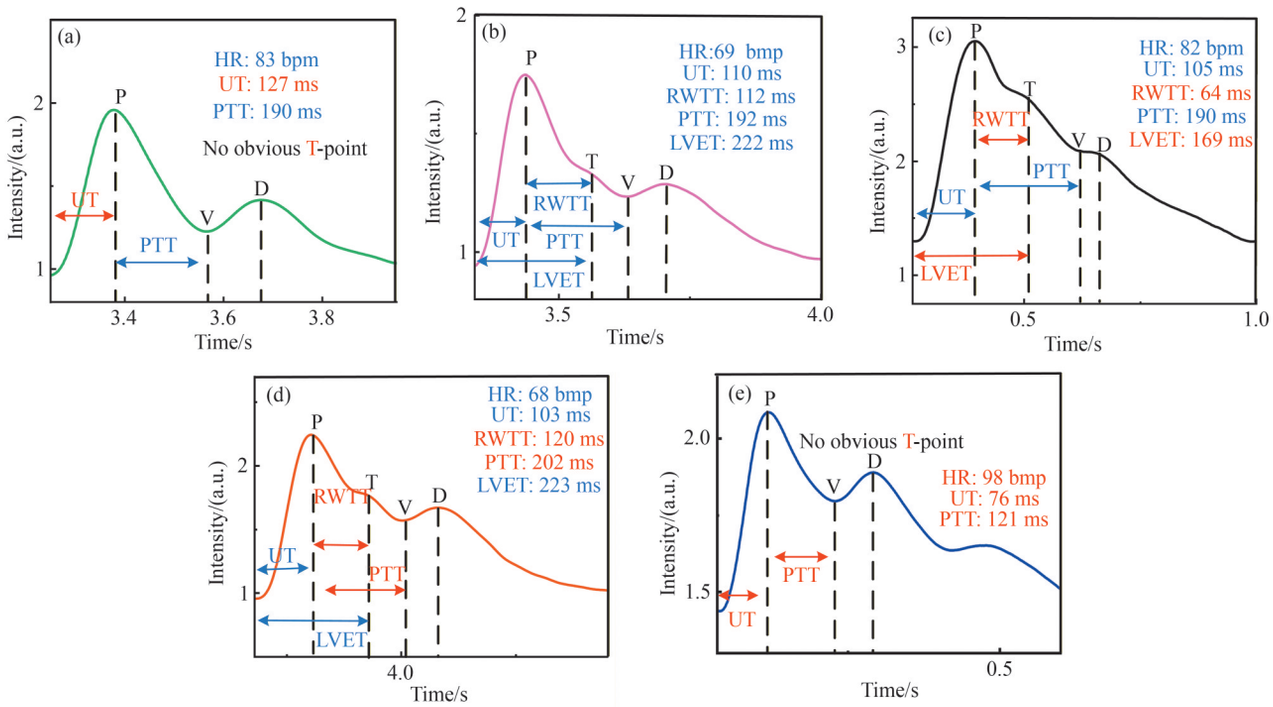


图9　基于波形分析的中医脉象客观化。(a)关部中候细脉的脉搏波形特征；(b)关部中候常脉的脉搏波形特征；(c)寸部中候紧脉的脉搏波形特征；(d)寸部中候滑脉的脉搏波形特征；(e)寸部中候数脉的脉搏波形特征

Fig. 9　Objectification of TCM Pulse Conditions based on Waveform Analysis. (a) Middle-thready pulse waveform characteristics in guan part; (b) Middle-normal pulse waveform characteristics in guan part; (c) Medium-tense pulse waveform characteristics in cun part; (d) Middle-slippery pulse waveform characteristics in cun part; (e) Medium-rapid pulse waveform characteristics in cun part

2.3　智能脉诊分析

尽管三通道传感器采集的脉搏波蕴含丰富的量化分析，但准确进行脉象分类仍面临诸多挑战，脉搏波既包含丰富的局部形态信息（如波峰、波谷等），也呈现复杂的时序动态和长期依赖关系。针对这一问题，提出一种基于深度学习的脉象分类方法，结合1D-CNN和BiGRU模型，直接从原始脉搏波信号中学习并区分不同脉象，如图10(a)所示。其中，1D-CNN层被用于高效提取脉搏波的局部形态特征；而BiGRU层则在此基础上，进一步建模信号的整体时序依赖和长期关联，从而全面捕捉脉象的关键判别信息，实现高精度分类。

为支持模型的训练与评估，本研究首先利用三通道MNF传感器采集“寸、关、尺”部位的原始脉搏波形数据；随后，在同一受试者的相应脉位，依次采用单通道蓝骄AI脉诊仪进行脉象分类，并将其分类结果作为模型训练的基准标签。在构建数据集阶段，充分考虑左右手的生理差异分别采集数据。选取6名男性和4名女性共10名参与者，在连续七天内，采集其左右手寸、关、尺三部位以及浮、中、沉三种按压状态下的脉搏波数据，每次采集时长约10 s。最终共获得1 260个样本的数据集，其脉象分布如下：常脉366个、实脉120个、数脉84个、洪脉108个、滑脉270个、紧脉216个、细脉96个。采集完成后，将数据集按70%训练集、15%验证集、15%测试集的比例划分，用于模型训练与性能评估。

在此基础上对模型进行训练与测试，重点关注其对左、右手七种常见脉象的识别效果。结果表明，当仅采用中候脉搏波进行识别时，左手准确率为91.92%，如图10(b)，右手为92.01%，如图10(c)；而结合浮、中、沉三候脉搏波数据后，左手准确率提升至96.61%，如图10(d)，右手达96.07%，如图10(e)。为全面展示本研究所提出的模型在脉象分类中的性能优势，表3比较不同深度学习模型在特征提取方式、样本规模、类别数量及分类准确率方面的表现。结果表明，1D-CNN与BiGRU结合的模型在相似样本规模条件下实现96.61%的最高准确率，优于依赖手工特征或单一网络结构的模型，验证其在脉象识别任务中的有效性与优越性。此外，根据中医理论，脉象与穴位及脏腑功能密切相关，寸、关、尺三部对应不同脏腑，不同脉象可反

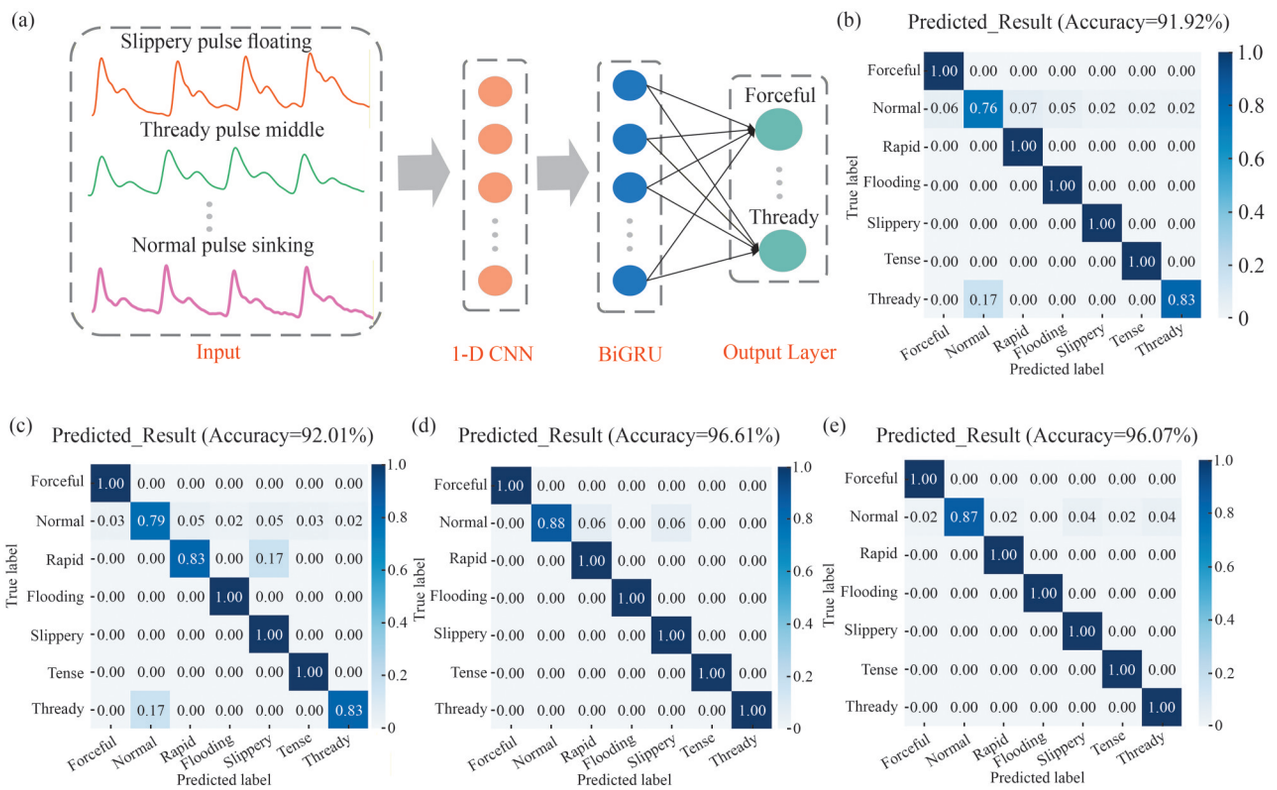


图 10 深度学习在脉象识别中的应用。(a)1-D CNN与BiGRU的神经网络结构;(b)左手中候识别的混淆矩阵;(c)右手中候识别的混淆矩阵;(d)左手浮、中、沉三候识别的混淆矩阵;(e)右手浮、中、沉三候识别的混淆矩阵

Fig. 10 The application of deep learning in pulse recognition. (a) Neural network structures of 1-D CNN and BiGRU; (b) Confusion matrix for identifying the middle pulse of left hand; (c) Confusion matrix for identifying the middle pulse of right hand; (d) Confusion matrix for identifying the "floating, middle and sinking" pulses in the left hand; (e) Confusion matrix for identifying the "floating, middle and sinking" pulses in the right hand

表 3 不同深度学习模型在脉象分类中的性能比较

Table 3 Comparison of the performance of different deep learning models in pulse classification

Model	Feature extraction	Sample size	Classes	Accuracy	References
CNN	End-to-end convolutional features	680	10	94.12%	[21]
DSSN	CNN features + handcrafted features	1 812	7	83.2%	[22]
FCN	Handcrafted time/frequency features	80	2	91%	[23]
1D-CNN + BiGRU	CNN local features + BiGRU temporal features	1 260	7	96.61%	This work

映相应脏腑病理[20],因此,本研究模型不仅提升脉象识别的准确率,还结合脉象与脏腑的对应关系,为中医诊断和脏腑健康状态的推断提供可靠依据。

3 结论

本文提出一种基于三通道U型MNF柔性传感器,用于高灵敏度脉搏波信号采集与脉象识别。通过模拟中医的寸、关、尺三部诊脉模式,精确采集"浮、中、沉"三候的脉搏信息,具有高灵敏度(11.49% kPa^{-1}、11.64% kPa^{-1}和11.13% kPa^{-1})、快速响应与恢复时间(22.7 ms/9.4 ms、31.2 ms/10.6 ms和29.8 ms/8.5 ms)、良好的一致性及重复性等优势。进一步将传统中医脉诊与现代生理定量分析方法相融合,利用深度学习模型,实现对左、右手典型脉象的高精度分类(96.61%和96.07%)。该传感器能够应用于中医脉诊实践,并在典型脉象分类任务中展现出优异性能,不仅为脉搏信号的客观化采集提供了一条新的途径,更在中医脉诊的客观化、数字化、远程诊疗及慢病管理等领域展现出应用潜力。

参考文献

[1] YU Xuan, WU Shouyuan, ZHANG Juanjuan, et al. Developing TCM clinical practice guidelines: a comparison between

traditional Chinese medicine and western medicine[J]. Integrative Medicine Research, 2023, 12(2): 100952.
[2] XI Zhichao, DAI Rongchen, ZE Yufei, et al. Traditional Chinese medicine in lung cancer treatment[J]. Molecular Cancer, 2025, 24: 57.
[3] MingLYU, FAN Guanwei, XIAO Guangxu, et al. Traditional Chinese medicine in COVID-19[J]. Acta Pharmaceutica Sinica B, 2021, 11(11): 3337-3363.
[4] TIAN Xin, CHENG Guanyin, WU Zhonghuai, et al. High-resolution carbon-based tactile sensor array for dynamic pulse imaging[J]. Advanced Functional Materials, 2024, 34(46): 2406022.
[5] WANG Shihang, ZHANG Zhinan, CHEN Zhijian, et al. Development of pressure sensor based wearable pulse detection device for radial pulse monitoring[J]. Micromachines, 2022, 13(10): 1699.
[6] QIN Jing, YIN Lijuan, HAO Yanan, et al. Flexible and stretchable capacitive sensors with different microstructures[J]. Advanced Materials, 2021, 33(34): 2008267.
[7] PANG Yaokun, XU Xianchen, CHEN Shoue, et al. Skin-inspired textile-based tactile sensors enable multifunctional sensing of wearables and soft robots[J]. Nano Energy, 2022, 96: 107137.
[8] QU Xuecheng, XUE Jiangtao, LIU Ying, et al. Fingerprint-shaped triboelectric tactile sensor[J]. Nano Energy, 2022, 98: 107324.
[9] LI Jihong, CHEN Jinhui, XU Fei. Sensitive and wearable optical microfiber sensor for human health monitoring[J]. Advanced Materials Technologies, 2018, 3(12): 1800296.
[10] PAN Jing, ZHANG Zhang, JIANG Chengpeng, et al. A multifunctional skin-like wearable optical sensor based on an optical micro-nano fibre[J]. Nanoscale, 2020, 12(33): 17538-17544.
[11] LI Liangye, LIU Yunfei, SONG Changying, et al. Wearable alignment-free microfiber-based sensor chip for precise vital signs monitoring and cardiovascular assessment[J]. Advanced Fiber Materials, 2022, 4: 475-486.
[12] ZOU Xue, FAN Junhao, LUO Binbin, et al. Dual-channel reflective optical microfiber coupler diaphragms for continuous and accurate blood pressure monitoring[J]. Acta Optica Sinica, 2024, 44(7): 0728001.
邹雪, 范俊豪, 罗彬彬, 等. 基于双通道反射式微纳光纤耦合器膜片的精准连续血压监测[J]. 光学学报, 2024, 44(7): 0728001.
[13] CHEN Zongyu, DONG Bo, SHAO Qi, et al. Flexible arc-shaped micro-fiber Bragg grating array three-dimensional tactile sensor for fingertip signals detection and human pulse monitoring[J]. ACS Applied Materials & Interfaces, 2024, 16(32): 42986-42994.
[14] QUAN Zhenxue. Discussion on the application of the cunkou sanbu jiuhou pulse method in shanghan lun based on the four elements of pulse and basic pulse[J]. Traditional Chinese Medicine News, 2023, 29(5): 76-79.
全贞雪. 基于脉象四要素和基础脉象探讨寸口三部九候脉法在《伤寒论》中的应用[J]. 中医药导报, 2023, 29(5): 76-79.
[15] WANG Zhijun, HUANG Shengyou, LI Kun, et al. Vocal cord vibration sensors and speech intelligent recognition based on s-shaped micro-nano optical fibers[J]. Acta Photonica Sinica, 2025, 54(5): 0506003.
王智君,黄嵘釉,李昆,等. 基于S型微纳光纤的声带振动传感器及语音智能识别研究[J]. 光子学报, 2025, 54(5): 0506003.
[16] FAN Chenglei, LUO Binbin, WU Decao, et al. Research on flexible bionic microstructure tactile sensors based on micro-nano fibers[J]. Acta Optica Sinica, 2023, 43(21): 2106004.
范成磊, 罗彬彬, 吴德操, 等. 基于微纳光纤的柔性仿生微结构触觉传感器研究[J]. 光学学报, 2023, 43(21): 2106004.
[17] HUANG Ling, LUO Binbin, ZOU Xue, et al. Research on efficient braille recognition based on the pair-U-shaped micro-nano optical fiber fingerprint-like tactile sensors[J]. Optics & Laser Technology, 2024, 179: 111349.
[18] LIU Kaijun, FAN Junhao, LUO Binbin, et al. Highly sensitive vibration sensor based on the dispersion turning point microfiber Mach-Zehnder interferometer[J]. Optical Express, 2021, 29(21): 32983-32995.
[19] GAO Lisha, LI Yan, YU Xiaofei, et al. Screening of traditional chinese medicine pulse differentiation indicators based on Doppler ultrasound technology[J]. Journal of Binzhou Medical College, 2024, 47(5): 385.
高丽莎, 李岩, 于晓飞, 等. 基于多普勒超声技术的中医脉象鉴别指标筛选[J]. 滨州医学院学报, 2024, 47(05): 385.
[20] XIANG Fengmei. My view on clinical pulse diagnosis[J]. Journal of Jiangxi University of Traditional Chinese Medicine, 2020, 32(2): 22-23.
项凤梅. 临床脉诊之我见[J]. 江西中医药大学学报, 2020, 32(2): 22-23.
[21] QuanyuE. Pulse signal analysis based on deep learning network[J]. BioMed Research International, 2022: 6256126.
[22] YAN Jianjun, CAI Xianglei, CHEN Songye, et al. Ensemble learning-based pulse signal recognition: classification model development study[J]. JMIR Medical Informatics, 2021, 9(10): e28039.
[23] LAN Kunchan, LITSCHER G, HUNG Tehsuan. Traditional chinese medicine pulse diagnosis on a smartphone using skin impedance at acupoints: a feasibility study[J]. Sensors, 2020, 20(16): 4618.

Research on Traditional Chinese Medicine Pulse Diagnosis Based on Three Channel U-shaped Micro Nano Fiber Pulse Sensor

LIU Zhihai, LUO Binbin, WU Decao, ZOU Xue, LI Kun, HUANG Shengyou, HU Xinyu
(*Chongqing Key Laboratory of Optical Fiber Sensor and Photoelectric Detection*, *Chongqing University of Technology*, *Chongqing* 400054, *China*)

Abstract: Pulse diagnosis, as a core diagnostic method in traditional Chinese medicine, has long faced challenges such as strong subjectivity and difficulty in standardization. To address these issues, this paper proposes a pulse diagnosis sensing system based on a tri-channel U-shaped Micro-Nano Fiber (MNF) sensor. The system can synchronously acquire pulse signals from the cun, guan, and chi positions at different pressing depths (floating, middle, and sinking), comprehensively capture subtle variations in pulse waveforms, and integrate deep learning models to achieve accurate pulse recognition, thereby enhancing the objectivity and digitization of traditional Chinese medicine diagnosis.

To construct a synchronous signal acquisition system, three well matched U-shaped MNFs were embedded in a Polydimethylsiloxane (PDMS) film and fixed on a Polycarbonate (PC) substrate to form sensing units, which were arranged on the cun, guan, and chi parts respectively. MNF was prepared using flame heating cone method, with a diameter of about 3 μm and a bending radius of 2 mm. Its structural parameters were optimized through COMSOL simulation to achieve a balance between evanescent field effect and mechanical strength, ensuring both adaptation to radial artery pulsation and stable and accurate detection. The PDMS package thickness was optimized through ANSYS finite element simulation and ultimately determined to be 100 μm to achieve the best balance between mechanical strength and sensitivity. Three sensing units are integrated into a customized 3D printed silicone platform, which has good biocompatibility and can adapt to individual physiological differences. In the experimental section, a tri-channel Photoelectric Detection (PD) module was used to convert the optical signals into electrical signals, and the dynamic waveforms were displayed in real time on an oscilloscope. To simulate the three pulse conditions of "floating, middle, and sinking" in traditional Chinese medicine, an airbag cuff loading system was designed to apply different levels of pressure to the pulse positions, thereby enabling signal acquisition. Through signal processing, multiple physiological parameters including Rise Wave Transit Time (RWTT), Upstroke Time (UT), Pulse Transit Time (PTT), Left Ventricular Ejection Time (LVET), etc. are extracted. In terms of intelligent recognition, a dataset containing 1 260 annotated pulse wave data was constructed, covering seven typical pulse types: normal pulse, forceful pulse, rapid pulse, flooding pulse, slippery pulse, tense pulse, and thready pulse. A deep learning model combining one-dimensional Convolutional Neural Network (1D-CNN) and Bidirectional Gated Recurrent Unit (BiGRU) is proposed, where CNN is used for local feature extraction and BiGRU is used to capture temporal dependencies, thereby achieving efficient classification of multi-channel pulse signals.

Mechanical performance tests show that the sensitivity of the three channel MNF sensor in the pressure range of 0~7 kPa is 11.49% kPa^{-1}、11.64% kPa^{-1} and 11.13% kPa^{-1}, respectively. The response time and recovery time are 22.7 ms/9.4 ms、31.2 ms/10.6 ms and 29.8 ms/8.5 ms, demonstrated favorable sensitivity and a high level of consistency. After 600 cycles of loading unloading, the signal remained stable, verifying the reliability of the packaging structure. Compared with existing flexible pulse sensors, this device has advantages in sensitivity, channel count, and response speed.In the pulse diagnosis experiment, the system can simultaneously obtain pulse signals from the cun, guan, and chi parts, and clearly characterize the waveform differences at different compression depths. As the pressure increases from shallow to deep, the pulse wave gradually flattens, UT shortens, and the rate of rise accelerates, indicating physiological changes in reduced vascular wall compliance. Through waveform analysis, objective parameters of seven common pulse patterns were successfully extracted, which were highly consistent with clinical manifestations in volunteer experiments. For example, diarrhea patients showed thready pulse, while cold patients showed tense pulse, demonstrating the effectiveness of the system in capturing pulse patterns. In the intelligent recognition experiment, the deep learning model achieved 91.92% and 92.01% accuracy in classifying left and right hand pulse signals, respectively, when only using intermediate data; When integrating data from floating, medium, and sinking phases, the accuracy significantly improves to 96.61% (left hand) and 96.07% (right hand). Compared with existing

classification methods based on manual features or single networks, this method exhibits higher classification performance on similar data scales, demonstrating the superiority of combining 1D-CNN and BiGRU in complex pulse recognition.

The flexible pulse diagnosis and perception system based on three channel U-shaped MNF proposed in this study can achieve synchronous acquisition of pulse waves from multiple parts and depths of compression, and combine deep learning to achieve high-precision pulse recognition. This method effectively improves the objectivity and standardization level of traditional Chinese medicine pulse diagnosis, and has broad application prospects in remote medical care, digital diagnosis and treatment, and chronic disease management.

Key words: Fiber optic sensor; Micro-nano fiber; Traditional Chinese medicine pulse diagnosis; Pulse recognition; Tri-channel

OCIS Codes: 060.2370; 060.4005; 120.5475; 100.4996

CSTR: 32255.14.gzxb20265501.0106006

Foundation item: Chongqing Natural Science Foundation Innovation and Development Joint Fund (CSTB2023NSCQ-LZX0008), Chongqing Municipal Education Commission Science and Technology Research Project (KJQN202401103), National Key Laboratory of Market Regulation Open Project (CQTJ-XBJD-KFKT202302), Chongqing University of Technology Innovation Team (2023TDZ002), Chongqing University of Technology Major Research Projects Simultaneously Carrying out Basic and Applied Basic Research (2024TBZ027)